Electrochemical Quartz Crystal Microbalance, Voltammetry, Spectroelectrochemical, and Microscopic Studies of Adsorption Behavior for (7*E*,7′*Z*)-Diphenyl-7,7′-diapocarotene Electrochemical Oxidation Product

Guoqiang Gao, David B. Wurm, Yeon-Taik Kim,† and Lowell D. Kispert*

Department of Chemistry, University of Alabama, Tuscaloosa, Alabama 35487-0336

Received: November 8, 1996; In Final Form: January 14, 1997[⊗]

Polymeric products, which are formed by reaction of the dications of (7*E*,7′*Z*)-diphenyl-7,7′-diapocarotene (**I**) generated by electrochemical oxidation in dichloromethane with the neutral carotenoid, are adsorbed on various electrode surfaces. An apparent average molar mass of 5400 g/(mol electrons) was calculated from simultaneous electrochemical quartz crystal microbalance (EQCM) measurements, and the green, fiber-like structure observed by optical microscopy confirms the formation of polymers. X-ray microanalysis of the surface composed of an uneven, layered structure indicates that electrolyte counter anions PF_6^- are associated with the deposited material. Cathodic stripping voltammetry indicates that the film thickness ranges from 0.16 to 0.84 μm as the charge increases from 10.0 to 51.1 μC. Cation radicals of **I** show no adsorption behavior nor do the dications of carotenoids terminally substituted with one cyclohexene ring (**V**) or containing a triple bond at C15 (**IV**). Apparently a diphenyl-substituted carotenoid containing only double bonds in the backbone is required to observe this unusual behavior.

Introduction

Carotenoids play important roles in photosynthetic systems as photoprotecting agents and light harvesting antenna pigments.[1−3] Of particular interest are the more recent findings that carotenoids also function as potent anticarcinogens for lung cancer[4,5] and several other types of cancer[6,7] and are good antioxidants capable of quenching free radicals[8−10] and other reactive chemical species such as singlet oxygen and triplet chlorophyll.[11−13] In addition, of the more than 600 carotenoids that have been isolated from natural sources,[14] about 50 are metabolically converted to vitamin A, which is essential for vision, cellular differentiation, and embryonic development. Carotenoid cation radicals also play an active role in photodriven electron transport processes[15−17] and may participate in the photosynthetic electron flow.[18−20] It is therefore important to determine the structure and properties of the various carotenoid species that are involved in biochemical, photochemical, and electrochemical processes. The structures of the carotenoids **I**−**V** used in this study are given below. Compounds **II** and **III** are common natural products; the others are synthetic.

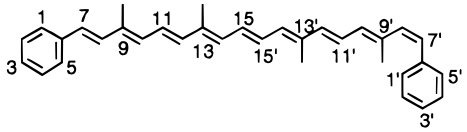

7*E*,7'*Z*-Diphenyl-7,7'-diapocarotene (I)

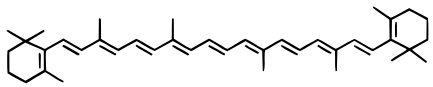

β-Carotene (II)

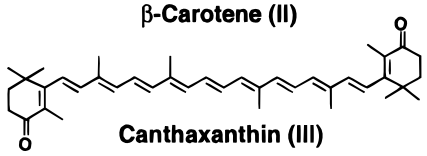

Canthaxanthin (III)

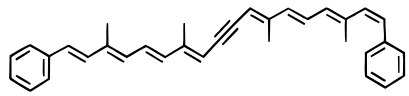

7*E*,7'*Z*-Diphenyl-15,15'-didehydro-7,7'-diapocarotene (IV)

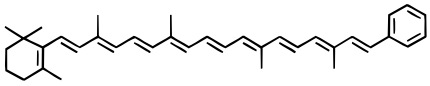

7'*E*-Phenyl-7'-apo-β-Carotene (V)

Methods such as polarography,[21,22] CV (cyclic voltammetry),[23−25] and SEEPR (simultaneous electrochemical and electron paramagnetic resonance) studies[24−27] have been employed to study the electrochemical behavior of carotenoids. The results reveal that during an electrochemical oxidation−reduction cycle not only cation radicals but also dications, cations (loss of one H^+ from dications), and neutral radicals can be formed. The electrode and homogeneous reactions in Scheme 1 have been identified.[25,28]

The electrochemical oxidation−reduction reactions of many carotenoids in dichloromethane are quasi-reversible or reversible, so that the CV displays comparable, symmetrical anodic and cathodic peaks.[26,27] For example, the CV of canthaxanthin (**III**) consists of two separate, comparable sets of waves ($\Delta E^\circ = E^\circ_2 - E^\circ_1 \approx 200$ mV), whereas the CV of β-carotene (**II**) shows only one set of waves because the two oxidation potentials are nearly the same ($\Delta E^\circ = E^\circ_2 - E^\circ_1 \approx 0$ mV). In contrast, the CV of (7*E*,7′*Z*)-diphenyl-7,7′-diapocarotene (**I**) displays an unexpected intense reduction peak current (Figure 1a, peak 3) that is much larger than the oxidation peak currents (Figure 1a, peaks 1 and 2). However, two other carotenoids, (7*E*,7′*Z*)-diphenyl-15,15′-didehydro-7,7′-diapocarotene (**IV**) and (7′*E*)-phenyl-7′-apo-β-carotene (**V**), although their structures are very similar to **I**, display very different CVs from that of **I** and show no enhanced reduction peak. We recently demonstrated by cyclic voltammetry and optical spectroscopy[29] that the enhanced reduction peak of **I** is due to adsorption of dications on the surface of the electrodes of various materials such as platinum,

* Author to whom correspondence should be addressed.
† Present address: Department of Chemistry, Yonsei University, Seoul, Korea.
⊗ Abstract published in *Advance ACS Abstracts,* February 15, 1997.

S1089-5647(96)03741-8 CCC: $14.00 © 1997 American Chemical Society

SCHEME 1

Electrode reactions

$$\mathrm{Car} \overset{E^\circ_1}{\rightleftharpoons} \mathrm{Car}^{\bullet+} + \mathrm{e}^- \quad (1)$$

$$\mathrm{Car}^{\bullet+} \overset{E^\circ_2}{\rightleftharpoons} \mathrm{Car}^{2+} + \mathrm{e}^- \quad (2)$$

$$*\mathrm{Car}^{\bullet} \overset{E^\circ_3}{\rightleftharpoons} *\mathrm{Car}^{+} + \mathrm{e}^- \quad (3)$$

Homogeneous reactions

$$\mathrm{Car}^{2+} + \mathrm{Car} \overset{K_{com}}{\rightleftharpoons} 2\mathrm{Car}^{\bullet+} \quad (4)$$

$$\mathrm{Car}^{2+} \overset{K_{dp}}{\rightleftharpoons} *\mathrm{Car}^{+} + \mathrm{H}^+ \quad (5)$$

$$\mathrm{Car}^{\bullet+} \overset{K'_{dp}}{\rightleftharpoons} *\mathrm{Car}^{\bullet} + \mathrm{H}^+ \quad (6)$$

where *Car represents the carotenoid with one less proton

gold, and glassy carbon, although the identity and molecular weight of the adsorbed material were not determined.

Simultaneous electrochemical quartz crystal microbalance (EQCM) measurements[30−33] constitute a sensitive probe for detecting mass changes down to *ca.* 10 ng occurring in liquid media on an electrode surface during, for example, electrodeposition or dissolution of metals, adsorption of anions, and formation of thin-film semiconductors, self-assembled monolayers, and redox and conducting polymers. The EQCM has become an extremely useful tool for investigating interfacial processes at surfaces and thin films in recent years.

In an EQCM, a thin quartz crystal is sandwiched between two metal electrodes to which an alternating electric field is applied to generate a vibrational motion at the quartz resonant frequency. This frequency, typically 5−10 MHz, depends on the mass (among other factors) of the assembly. Since one of the electrodes can be used as the working electrode in an EQCM experiment, any increase (decrease) in mass resulting from electrodeposition (desorption) will result in a change (decrease/increase) in the resonant frequency of the crystal.

In this study the EQCM technique was employed to directly monitor the mass changes that occurred during electrodeposition of the reaction products of the dication of **I**. The simultaneous CV and the large apparent molar mass of deposited materials calculated from the decrease in the resonant frequency suggest that dications initiate the formation of polymer films. Optical and scanning electron microscope images were taken of the films deposited on the gold surface. Cathodic stripping voltammetry was carried out to determine the quantitative relationship of peak potential with film thickness.

It is relevant to note that a series of compounds similar to **I**, diphenylpolyenes containing 1−8 conjugated double bonds and used as models or oligomers of the conjugated polymers, have been extensively studied to determine their electronic structure,[34,35] charge storage and conductivity after doping,[36,37] optical spectra,[38,39] and radical structure.[40,41] *tert*-Butyl-capped polyenes containing 3−13 conjugated double bonds have also been thoroughly studied by T. Bally et al.[42] to determine the nature of the polaron structure in conjugated polyenes. The study of oligomers of conjugated polymers is attracting increasing interest because these materials can be exploited in applications such as the all-organic transistor developed by Garnier et al.[43] The unique electrochemical and polymeric nature of the title carotenoid of this study therefore is of fundamental interest not only to photochemical, biochemical, and electrochemical processes but also because it bridges the gap between the conjugated polymers and the shorter conjugated polyenes.

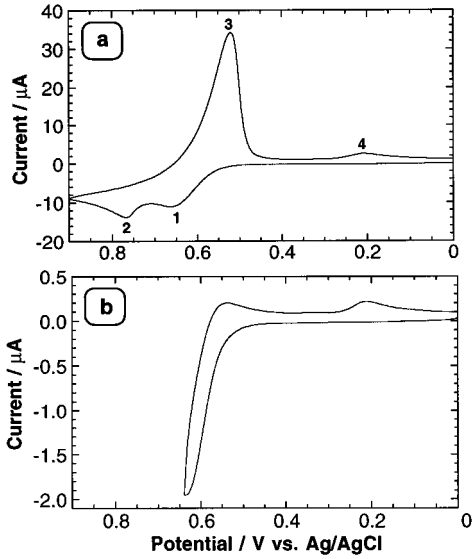

Figure 1. (a) CV of 1 mM solution of (7*E*,7′*Z*)-diphenyl-7,7′-diapocarotene (**I**), 0.1 M TBAHFP, dichloromethane, scan rate 0.1 V s^{-1}, and reversal at 0.9 V. (b) Same as (a), but scan rate 0.025 V s^{-1} and scan reversal at 0.65 V. Working electrode is platinum.

Experimental Section

(7*E*,7′*Z*)-Diphenyl-7,7′-diapocarotene (**I**), (7*E*,7′*Z*)-diphenyl-15,15′-didehydro-7,7′-diapocarotene (**IV**), and (7′*E*)-phenyl-7′-apo-β-carotene (**V**) were synthesized as previously described.[44] Tetrabutylammonium hexafluorophosphate (TBAHFP) was purchased from Fluka. Anhydrous dichloromethane was obtained from the Aldrich Chemical Co. All solutions were prepared in a drybox under a nitrogen atmosphere. Except as specifically noted, the dichloromethane solutions were 1 mM in **I** and 0.1 M in TBAHFP.

The EQCM was built in the laboratory and controlled by a PC computer through a homemade interface board.[45] AT-cut quartz crystals (10.0 MHz) coated with gold were purchased from International Crystal Manufacturer Inc., Oklahoma City, OK. The area of the gold electrode exposed to the solution was 0.27 cm^2. Ag/AgCl and Pt wire were used as reference and counter electrodes, respectively.

Voltammetry and other electrochemical experiments were carried out using the Bio Analytical Systems BAS-100W electrochemical analyzer. For voltammetry, a platinum disk electrode (0.07 cm^2) was used. The disk electrode was polished by using first 1 μm polishing alumina and then 0.05 μm polishing alumina. The reference electrode was a Ag/AgCl electrode with 3 M NaCl; the counter electrode was a platinum wire.

Optical absorption spectra in the range 190−1100 nm were measured using a Shimadzu UV-1601 UV−visible spectrophotometer. For simultaneous bulk electrolysis and optical absorption spectroscopic measurement, a transparent glass plate (1 × 3 cm^2) coated with InO_2/SnO_2 (ITO) served as the working electrode, and silver and platinum wires were used as pseudo-reference and counter electrodes, respectively. The electrochemical cell,[46,47] divided into two compartments by a frit, was equipped with requisite quartz windows and used for simultaneous bulk electrolysis and optical measurements. A 10 mL cylindrical undivided cell was used for CV measurements and electrodeposition of **I** on a gold-coated glass plate for microscope and X-ray microanalyses.

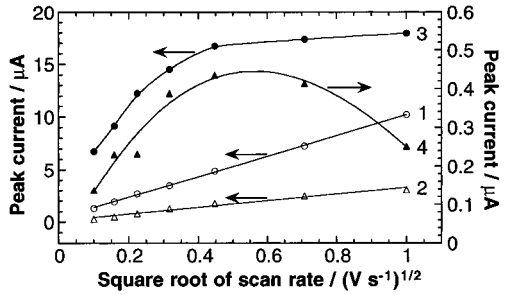

Figure 2. CV peak current vs square root of scan rate of (1) peak 1, (2) peak 2, (3) peak 3, and (4) peak 4. Same conditions as in Figure 1.

Electron microscope images and X-ray microanalysis were obtained with a S-2500 HITACHI scanning electron microscope equipped with a NORAN (Tracor Northern) energy dispersive X-ray analysis unit.

Results and Discussion

Cyclic Voltammetry. The CV of **I** obtained with a platinum disk electrode (Figure 1a) shows that during the anodic scan there are two waves, which correspond to the two one-electron oxidations of the neutral species and the resulting cation radical. During the cathodic scan, however, in the region where two waves corresponding to the reduction of the dication and the cation radical should have occurred, only a single, greatly enhanced wave is observed. [Wave 4 results from the reduction (reverse of eq 3) of the transient intermediate $*Car^{+}$.] The enhanced reduction wave 3 is due to adsorption or electrodeposition of species formed only after the generation of the dications of **I**,[29] not involving cation radicals, as evidenced by a CV (Figure 1b) in which the scan was reversed at the peak potential of the first wave (0.65 V), prior to the formation of dications. The intense reduction wave 3 is absent; however, wave 4 is still present. Further, the fact that this CV (Figure 1b) is essentially irreversible indicates that the cation radical is highly unstable, and this may be due to a fast deprotonation reaction of the cation radical (eq 6) with Cl^{-} as the possible proton acceptor. The $*Car^{\bullet}$ species resulting from the deprotonation of the cation radical is oxidized, forming $*Car^{+}$ (eq 3) at the potential of wave 1. $*Car^{+}$ is then reduced at wave 4 to form $*Car^{\bullet}$. CVs performed by further cycling for six times show no significant change. A 10-fold dilution results in similar adsorption behavior.

The relationship between the CV peak current and the scan rate is given in Figure 2. The currents of anodic peaks 1 and 2 exhibit a linear dependence on the square root of the scan rate (Figure 2, curves 1 and 2); the currents of the other two peaks show a marked nonlinear dependence (Figure 2, curves 3 and 4). This behavior indicates that peaks 1 and 2 are diffusion controlled; peak 3 is controlled by adsorption (curve 3); peak 4 is a typical kinetic-controlled one, as the current has a maximum at a specific scan rate (curve 4).

Electrochemical Quartz Crystal Microbalance (EQCM) Measurements. The CV of **I** and the simultaneously recorded EQCM frequency response Δf are illustrated in Figure 3a,b, respectively. During the forward scan (oxidation), frequency changes were observed only near the potential of the second wave; that is, the first electron oxidation induced no mass change, but the second electron oxidation produced significant mass loading. This observation supports the above conclusion that only the second electron oxidation is accompanied by electrodeposition.

During the reverse scan (reduction) the frequency difference Δf continued to decrease until the potential was less than the peak potential of the first wave. Below this value, Δf began to increase and was finally restored to its initial value where no material is deposited, indicating that desorption is complete.

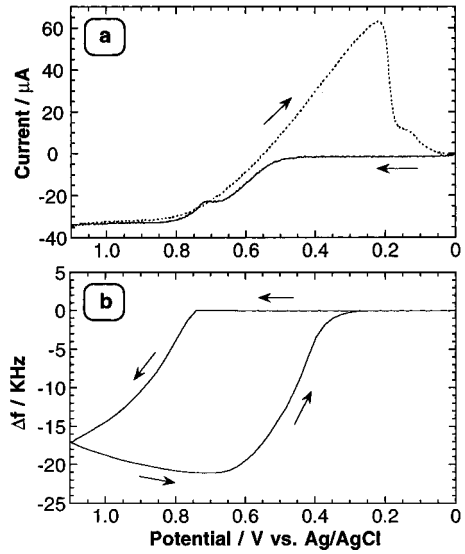

Figure 3. (a) CV of 1 mM solution of compound **I** in dichloromethane with 0.1 M TBAHFP, gold working electrode, scan rate 0.020 V s^{-1}. (b) Simultaneously recorded frequency shift of the AT-cut quartz crystal.

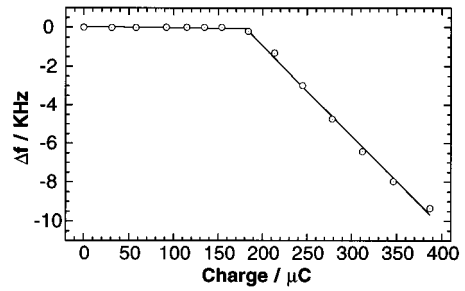

Figure 4. Frequency shift vs simultaneous charge transfer, data from Figure 3.

The change of the resonant frequency of the quartz crystal (Δf) depends on the deposited mass, and this, in turn, depends on the transferred charge Q, which is obtained by integration of the CV curve and converting potential to time by use of the known scan rate. The dependence of Δf on increasing Q during the oxidation (Figure 4) shows that electrodeposition occurred only after 184 μC had been applied and that further increase in Q results in a linear decrease ($r = 0.998$) in f.

The mass loading (Δm in g) is related to the measured frequency shift (Δf in Hz) by the Sauerbrey[48] equation (7) during the electrochemical process,[33,49−51] assuming that the film behaves as an elastic layer:

$$\Delta f = (-2.264 \times 10^{-6}) f_0^{\,2} \Delta m / S \qquad (7)$$

In equation 7, f_0 (Hz) is the fundamental resonant frequency of the unloaded quartz crystal, S (cm^2) is the area of the electrode surface, and the numerical constant is a combination of various constants, including the shear modulus and density of quartz. Substitution of Δm with the other parameters in the Faraday law gives eq 8:

$$\Delta f = (-2.264 \times 10^{-6}) f_0^{\,2} QM / nFS \qquad (8)$$

where Q (C) is the charge related to mass deposition, M (g mol^{-1}) is the apparent molar mass of deposited species, n is the number of electrons transferred, and F (96485.3 C/mol) is the Faraday constant. Equation 8 shows that the apparent molar

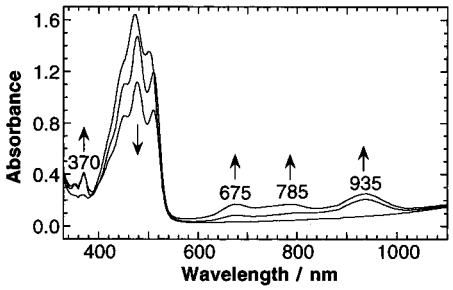

Figure 5. Optical absorption spectra obtained while simultaneously electrolyzing a 14 μM solution of **I** and 0.1 M TBAHFP in dichloromethane at 0.9 V for 0, 3, and 10 min, using an ITO electrode.

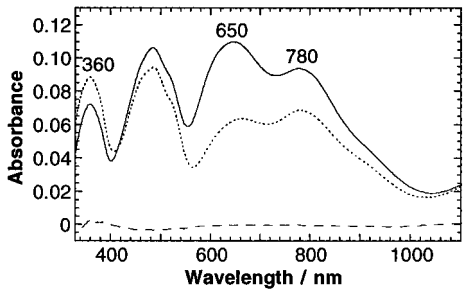

Figure 6. Spectra of material deposited on the ITO electrode: (solid line) immediately after electrolyzing the same solution as in Figure 5 for 3 min; (dotted line) 1 h after solid line; (dashed line) bare ITO.

mass M can be easily obtained when the frequency Δf varies linearly with the charge Q passed during the electrochemical process.

Evaluation of M and using the slope in Figure 4 for $\Delta f/Q$ (-4.7×10^7 Hz C^{-1}) gives 5400 g for the apparent average deposition mass per mole of electrons. Since this mass corresponds to about 12 monomeric units of molecule **I** (444.6 g mol^{-1}), it suggests that polymerization initiated by dications occurred during this electrochemical process. However, since two electrolyte (TBAHFP) counter anions (PF_6^-, 145 g mol^{-1}) are believed to be associated with the electrodeposition, the actual polymeric number is about 11. The presence of P and F was confirmed by X-ray microanalysis (see below). It appears that the polymerization number is nearly a constant throughout the deposition process. The effective surface of the electrode remains large even after a long deposition time due apparently to the conducting nature of the polymer formed.

Spectral Absorption and Optical Microscope Studies. Bulk electrolysis using an ITO electrode and simultaneous optical absorption measurements in the range 300−1100 nm were carried out in attempts to identify the adsorbed product. During bulk electrolysis of **I** at 0.9 V for 3 and 10 min, a green material formed a film on the electrode surface. A solution optical spectrum obtained (Figure 5) prior to electrolysis showed only the absorption of neutral **I** at 480 nm. After bulk electrolysis, three additional peaks with maxima at 675, 785, and 935 nm appeared, and their intensity increased as the electrolysis time was increased. As reported earlier,[29] the 935 nm absorption band is due to cation radicals of **I**, and the 675 nm band may be ascribed to dications of **I**. The 785 nm band may be due to the polymeric species formed during the electrochemical process.

After termination of the electrolysis, the ITO electrode was allowed to dry in the air for about 10 s, and spectra of the deposited solids were then determined. The solid line in Figure 6 shows that little, if any, of the cation radical (935 nm) is present in the deposited material. This observation is consistent with the conclusion of CV and EQCM experiments that the first

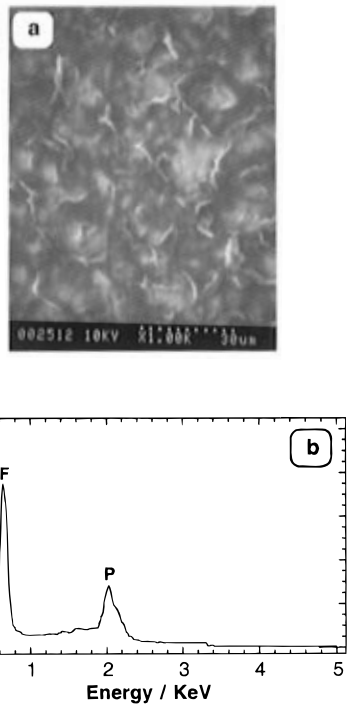

Figure 7. (a) Scanning electron microscopic image of film formed by electrolysis at 0.9 V for 5 min of a solution of **I** (1 mM in dichloromethane with 0.05 M TBAHFP). Magnification ×1000; 10 kV. (b) X-ray microanalysis of the same film, 5 kV. The three peaks were identified as due to carbon, fluorine, and phosphorus.

electron oxidation produces no adsorption or deposition. The two bands near 650 and 780 nm (Figure 6, solid line) are attributed to the deposited materials, which are relatively unstable. Thus, their intensities decreased after the ITO plate had been kept for an hour in the dark but in the presence of air (Figure 6, dotted line). Another band at 360 nm increased and is presumably due to the final products from decomposition of the deposited materials.

To determine the morphology of the deposited substances, optical microscopic images of the films on a gold-coated glass surface were taken. A film, prepared by casting a CH_2Cl_2 solution of neutral compound **I** and TBAHFP on the gold surface and then evaporating the solvent, displays a yellow homogeneous structure. The image of the film formed by electrodeposition of **I** is quite different. The color is then green, and a fiber-like web extends over the whole surface. This may indicate that polymeric species are formed during the electrochemical oxidation.

Scanning Electron Microscope and X-ray Microanalysis. Scanning electron microscope images of the film formed on a gold-coated glass surface by electrodeposition of **I** (Figure 7a) showed a rough surface containing flat regions surrounded by hills. The average diameter of the pits is around 10 μm. A layered structure can be recognized in the SEM images.

X-ray microanalysis of the same surface showed the presence of phosphorus and fluorine in the deposited materials (Figure 7b), indicating that electrolyte counter anions PF_6^- are associated with the formed polymeric species and coadsorbed on the electrode. PF_6^- tends to associate with some counter ions; for example, formation of contact ion pairs between diphenylpolyene radical cations and PF_6^- in dichloroethane solution has been reported.[40]

Electropolymerization Mechanism and AM1 MO Calculations. According to the above, polymeric species are formed during the electrochemical oxidation of **I**. A possible EEC mechanism is shown in Scheme 2.

SCHEME 2

$$\mathrm{Car}_{\mathrm{soln}} \xrightarrow{E^\circ_1} \mathrm{Car}^{\bullet+}{}_{\mathrm{soln}} + \mathrm{e}^- \quad (1)$$

$$\mathrm{Car}^{\bullet+}{}_{\mathrm{soln}} \xrightarrow{E^\circ_2} \mathrm{Car}^{2+}{}_{\mathrm{soln}} + \mathrm{e}^- \quad (2)$$

$$\mathrm{Car}^{2+}{}_{\mathrm{soln}} + \mathrm{Car}_{\mathrm{soln}} \rightarrow [\mathrm{Car{-}Car}]^{2+}{}_{\mathrm{soln}} \quad (9)$$

$$[\mathrm{Car{-}Car}]^{2+}{}_{\mathrm{soln}} + n\mathrm{Car} + 2\mathrm{PF_6}^- \rightarrow \mathrm{Products}_{\mathrm{ads}} \quad (10)$$

The final polymeric products are reducible as demonstrated by the CV of **I** (Figure 1a). Steps 9 and 10 indicate that as soon as the dications are formed, they react with neutral carotenoid molecules near the electrode surface, resulting in more rapid depletion of the reactant than in the absence of polymerization. This is consistent with the fact that peak 2 is smaller than peak 1 in Figures 1 and 2.

AM1 (Austin Model 1) semiempirical molecular orbital calculations of excess charge and bond length of the neutral, cation radical, and dication species of **I** were carried out on AM1-RHF geometry optimized structures using HyperChem software[52] running on a Gateway 2000 P5−60 (Pentium) personal computer. For the neutral species, as illustrated by the dotted line in Figure 8a, the excess charges at both the polyene backbone and phenyl group carbon atoms are all negative and alternate with small variation in a regular manner. In the cation radical (solid line, Figure 8a), however, larger variations of the excess charge are calculated and more positive charge is located at specific positions like C7, C9, C11, and C13. Even more dramatic changes occur in the dication (solid line, Figure 8b), and the excess charge at these mentioned four carbons remains more positive.

Figure 9 illustrates the alternation of the bond lengths among the backbone carbon atoms. In the neutral species (dotted line, Figure 9) the double and single bonds alternate in a regular manner somewhat similar to that found for polyenes.[36,37] However, dramatic changes occur in the dication (solid line, Figure 9) where the bond orders are inverted in the central part of the backbone, and the change in bond length gradually decreases toward both ends. In summary, the structure of the dication of **I** is shown as below.

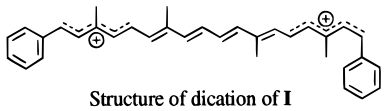

Structure of dication of **I**

The dication has a soliton-like structure where the positive charges are delocalized among C7−C11 (C7′−C11′), resulting in significant structural (bond length) relaxation. This charged soliton structure is stabilized by the two terminal phenyl groups. Charge storage and conductivity character of charged solitons formed from diphenylpolyenes on the polyene part of the molecule have been previously discussed.[36,37] Formation of charged soliton of β-carotene upon p-doping by intermolecular charge transfer has also been reported.[53] Solitons in conducting conjugated polymers have been detailed in ref 54. These observations are important for examining reactions in the current studies.

Since, according to AM1 calculations, C7 and C9 (C7′ and C9′) bear the largest positive charge, reaction might involve these carbon atoms; in other words, reaction occurred in the polyene backbone, not in the phenyl groups. However, C7 (C7′)

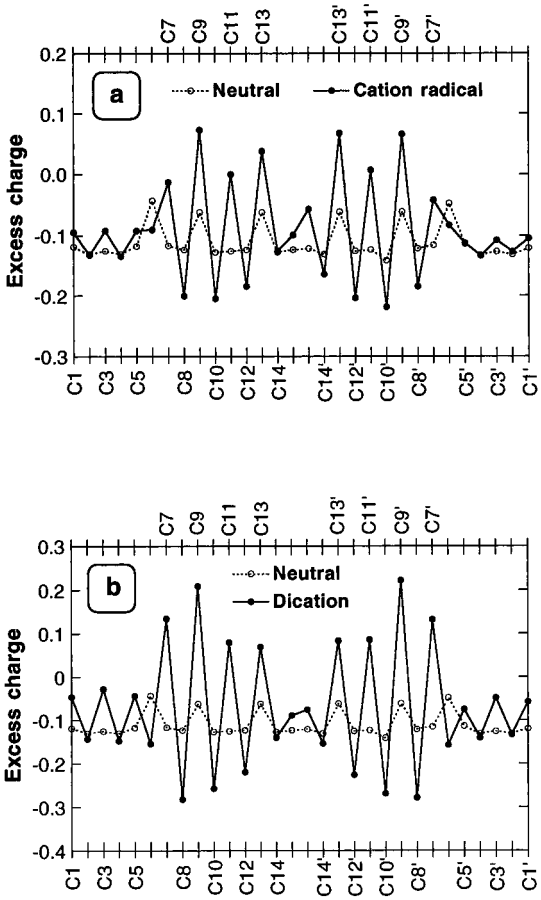

Figure 8. AM1 calculation of excess charge at both the polyene backbone and phenyl group carbon atoms of **I**. Dotted lines are neutral carotenoids in both a and b; solid line is cation radical in a and dication in b.

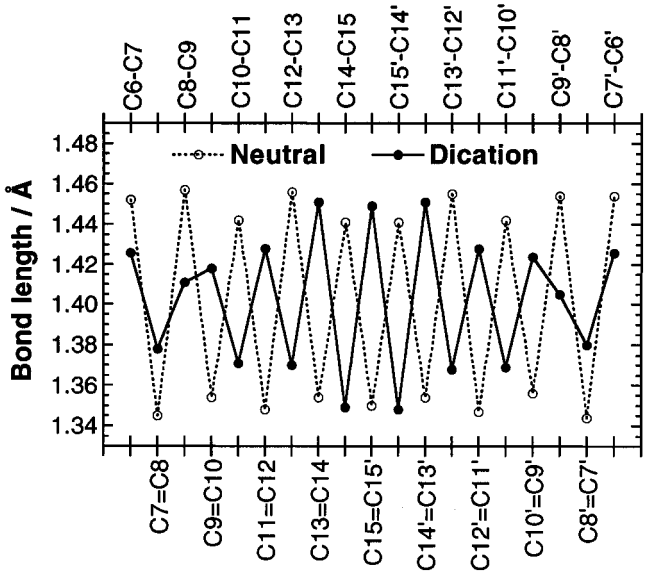

Figure 9. AM1 calculation of polyene backbone bond length of **I**. Dotted line is neutral carotenoid; solid line is dication.

is the preferred reaction site if steric factors are considered. A possible polymerization reaction, involving charge delocalization and soliton motion, is shown in Scheme 3.

C7′ of the dication of **I** attacks a neutral molecule of **I** and forms a dimer through a single bond perhaps between C7′ and C7; concurrently the positive charge is transferred to the other half of the dimer and moves to the "new" end, at which further polymeric reaction occurs until, as has been discussed in the

SCHEME 3

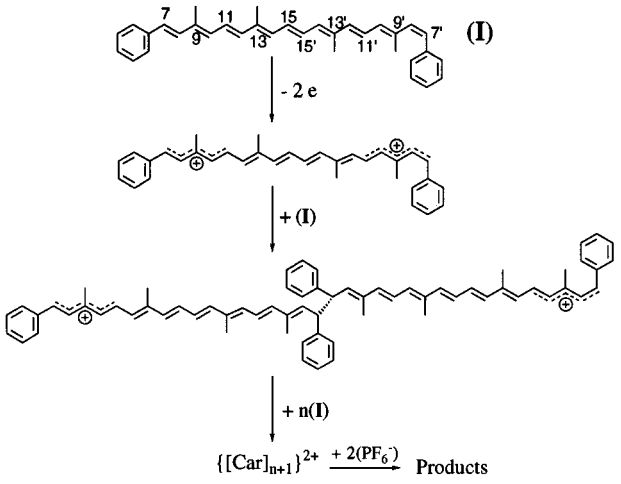

previous sections, an average of about 11 monomers of **I** link together. The charges of the polymer dication are counterbalanced by two PF_6^- anions present in the solution.

Comparison with Compounds IV and V. The electrochemical behavior of two other very similar compounds, (7*E*,7′*Z*)-diphenyl-15,15′-didehydro-7,7′-diapocarotene (**IV**) and (7′*E*)-phenyl-7′-apo-*β*-carotene (**V**), has been discussed elsewhere.[25,55] It is interesting that their CVs (Figure 10) are very different from that of **I** (Figure 1) and show no evidence of adsorption and/or polymerization. Such behavior can be readily interpreted by the mechanism in Scheme 3. For compound **V**, which bears only one terminal phenyl group, the polymerization reaction, if any, would stop at the second step (formation of dimer) since the methyl groups of the terminal cyclohexenyl group hinder reaction at C7. For compound **IV**, the central triple bond in the backbone interferes with the movement of the positive charge, so it is difficult to form a charged dimer soliton (Scheme 3). Further, as evidenced by the nearly irreversible CV reported previously,[55] dications of **IV** are quite unstable. It may also be noted that a central triple bond increases the oxidation potential by about 200 mV,[55] indicating that **IV** is more difficult to oxidize and is expected to be less reactive than **I**.

Cathodic Stripping Voltammetry Study of the Film Thickness. Cathodic stripping voltammograms of **I** indicate that with increasing deposition time from 2 to 50 s at 0.8 V both peak current and peak area (charge) increase (Figure 11a). Both quantities vary linearly with the square root of deposition time (Figure 11b).

Figure 11a also shows that the peak potentials shift to lower values as the amount of deposited substance increases, indicating that thin films were formed on the electrode surface. According to theory, the relationship between peak potential (E_p) and the thickness of a thin film (L) can be described by the following equation:[56]

$$n(E_p - E_{1/2}) = 1.43 - 29.58 \log\frac{L^2 \nu n F}{RTD} \qquad (11)$$

where υ is the kinetic viscosity, D is the diffusion coefficient, and other terms have their usual meaning. Equation 11 predicts that, when other parameters are fixed, E_p would shift to lower potential (for reduction) linearly with $\log(L^2)$.

An estimate of the deposited thin-film thickness can be made from the apparent deposition molar mass and the charge transfer related to deposition or desorption of the adsorbed species. The

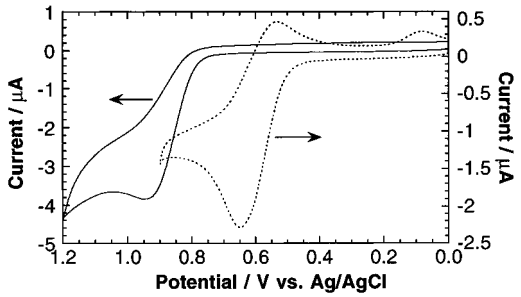

Figure 10. CVs of 1 mM solution of compounds **IV** (solid line) and **V** (dotted line), 0.1 M TBAHFP, dichloromethane, scan rate 0.05 V s^{-1}, starting at 0 V.

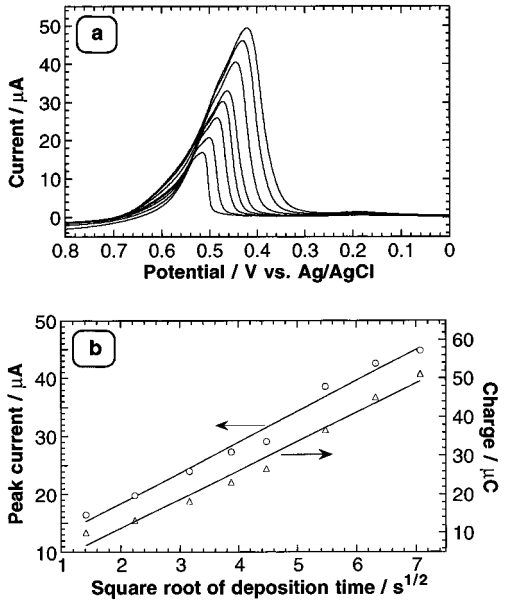

Figure 11. (a) Cathodic stripping voltammograms of 0.7 mM **I** in dichloromethane with 0.1 M TBAHFP, deposition at 0.8 V for 2, 5, 10, 15, 20, 30, 40, and 50 s before scanning at the rate of 0.1 V s^{-1}. (b) Plots of peak current (○) and peak area (△, charge) vs square root of deposition time. Working electrode is platinum.

number of molecules (assume monomer of **I**) can be calculated as follows:

$$\text{number of molecules} = \frac{QMN_A}{FM_0} \qquad (12)$$

where N_A is the Avogadro constant (6.0221×10^{23} mol^{-1}), M is the apparent deposition molar mass (5400 g/(mol electrons)), Q is the charge related to deposition or desorption (C), and M_0 is the molar mass of the monomer (444.6 g/mol).

If the deposited substances are homogeneously distributed on the surface and the distance between molecules is ignored, the thickness of the film can be expressed by

$$L = \frac{QMN_A}{FM_0}\frac{V}{S} \qquad (13)$$

where V is the volume of the molecule of **I** (cm^3/molecule), S is the area of the electrode surface (0.07 cm^2), and L is the film thickness (cm).

The volume of **I** is 1527.4 $Å^3$/molecule as estimated from the QSAR (quantitative structure−activity relationships) properties calculation using ChemPlus software[57] running on a Gateway 2000 P5-60 (Pentium) personal computer. The structure of the neutral molecule **I** was first geometry optimized by AM1 calculations.

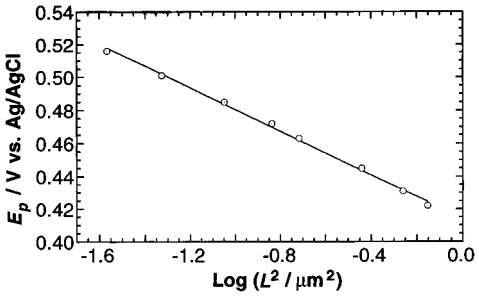

Figure 12. Peak potential as a function of log(L^2); data from Figure 11a and Table 1.

TABLE 1: Thickness of Thin Film Formed by Electrodeposition Estimated from Data in Figure 11a

Q (μC)	L (μm)
10.02	0.16
13.24	0.22
18.22	0.30
23.23	0.38
26.68	0.44
36.66	0.60
45.10	0.74
51.08	0.84

The estimated L values (Table 1) range from 0.16 to 0.84 μm as the charge increases from 10.02 to 51.08 μC. Thus, by controlling the deposition time, the thickness of the film can be controlled.

As shown by a plot of E_p vs log (L^2) (Figure 12), the peak potential shows a linear dependence on film thickness, which is in good agreement with eq 11 for the film electrode. The above discussion indicates that stripping voltammetry is very useful for diagnosing thin films formed by electrochemical adsorption/deposition.

Conclusions

(7*E*,7′Z)-Diphenyl-7,7′-diapocarotene (**I**) dications generated by electrolysis in dichloromethane initiate polymerization with the neutral molecules of **I**, and the products are adsorbed on various electrodes. The cation radicals show no adsorption behavior and decay rapidly. Results of simultaneous electrochemical quartz crystal microbalance experiments confirm the above conclusion and give an apparent molar mass of 5400 g/(mol electrons). Optical microscopic images of the thin film formed by electrodeposition of **I** on a gold surface show a green fiber-like structure, supporting the assumption that polymeric species are formed by electrochemical oxidation. X-ray microanalysis of the film suggests that the electrolyte counter anions PF_6^- are associated with the electrodeposition. Similar carotenoids containing one terminal trimethylcyclohexene substituent (**V**) or a triple bond at C15 (**IV**) show no adsorption and/or polymerization behavior, indicating a diphenyl-substituted carotenoid is required to observe this unusual behavior, a feature important to the overall understanding of the oxidation and reduction properties of carotenoids.

Acknowledgment. We thank Dr. Elli Hand for synthesizing the carotenoids **I**, **IV**, and **V** and stimulating discussions. Lolanta Nenley is thanked for carrying out X-ray microanalysis and taking electron microscopic images. Q. Ren is thanked for help in obtaining the optical microscope images. We also express our gratitude to Hoffmann-La Roche Ltd., Basel, Switzerland, for a generous gift of the dialdehyde precursors to **I** and **IV**. This work was supported by the Division of Chemical Sciences, Office of Basic Energy Sciences of the U.S. Department of Energy, under Grant No. DE-FG05-86-ER13465.

References and Notes

(1) Goedheer, J. C. *Annu. Rev. Plant Physiol.* **1972**, *21*, 87.
(2) Koyama, Y. *J. Photochem. Photobiol.* **1991**, *B9*, 265.
(3) Frank, H. A.; Violette, C. A.; Trautman, J. K.; Shreve, A. P.; Owens, T. G.; Albrecht, A. C. *Pure Appl. Chem.* **1991**, *63*, 109.
(4) Ziegler, R. G. *J. Nutr.* **1989**, *119*, 116.
(5) Ziegler, R. G. *Am. J. Clin. Nutr.* **1991**, *53*, 251S.
(6) Malone, W. F. *Am. J. Clin. Nutr.* **1991**, *53*, 305S.
(7) Weisburger, J. H. *Am. J. Clin. Nutr.* **1991**, *53*, 226S.
(8) Burton, G. W.; Ingold, K. U. *Science* **1984**, *224*, 569.
(9) Krinsky, N. I. *Free Radical Biol. Med.* **1989**, *7*, 617.
(10) Palozza, P.; Krinsky, N. I. In *Methods in Enzymology*; Packer, L., Ed.; Academic Press, Inc.: CA, 1992; Vol. 213, p 403.
(11) Cogdell, R. J. In *Plant Pigments*; Goodwin, T. W., Ed.; Academic Press: New York, 1988.
(12) Foote, C. S. In *Free Radicals and Biological Systems*; Pryor, W. A., Ed.; Academic Press: New York, 1976; pp 85−133.
(13) Mathis, P.; Vermeglio, A. *Biochim. Biophys. Acta* **1975**, *369*, 371.
(14) Straub, O. In *Key to Carotenoids*; Pfander, H. P., Ed.; Birkhäuser Verlag: Basel, 1987.
(15) Seta, P.; Bienvenue, E.; Moore, A. L.; Mathis, P.; Bensasson, R. V.; Liddell, P.; Pessiki, P. J.; Moore, T. A.; Gust, D. *Nature (London)* **1985**, *316*, 653.
(16) Gust, D.; Moore, T. A.; Moore, A. L.; Makings, L. R.; Seely, G. R.; Ma, X.; Trier, T. T.; Gao, F. *J. Am. Chem. Soc.* **1988**, *110*, 7567.
(17) Gust, D.; Moore, T. A.; Moore, A. L.; Lee, S. J.; Bittersmann, E.; Luttrull, D. K.; Rehms, A. A.; DeGraziano, J. M.; Ma, X. C.; Gao, F.; Belford, R. E.; Trier, T. T. *Science* **1990**, *248*, 199.
(18) Schenck, C. C.; Diner, B.; Mathis P.; Satoh, K. *Biochim. Biophys. Acta* **1982**, *680*, 216.
(19) Mathis, P.; Rutherford, A. W. *Biochim. Biophys. Acta* **1984**, *767*, 217.
(20) Telfer, A.; Rivas, J. De Las; Barber, J. *Biochim. Biophys. Acta* **1991**, *1060*, 106.
(21) Takahashi, R.; Tachi, I. *Agr. Biol. Chem.* **1962**, *26*, 771.
(22) Takahashi, R. *Rev. Polarogr.* **1961**, *9*, 247.
(23) Mairanovsky, V. G.; Engovatov, A. A.; Ioffe, N. T.; Samokhvalov, G. I. *J. Electroanal. Chem.* **1975**, *66*, 123.
(24) Khaled, M.; Hadjipetrou, A.; Kispert, L. D. *J. Phys. Chem.* **1991**, *95*, 2438.
(25) Jeevarajan, A. S.; Khaled, M.; Kispert, L. D. *J. Phys. Chem.* **1994**, *98*, 7777.
(26) Khaled, M. Ph. D. Dissertation, University of Alabama, Tuscaloosa, 1992.
(27) Cheng, X. Master Thesis, University of Alabama, Tuscaloosa, 1991.
(28) Jeevarajan, J. A.; Kispert, L. D. *J. Electroanal. Chem.* **1996**, *411*, 57.
(29) Gao, G.; Jeevarajan, A. S.; Kispert, L. D. *J. Electroanal. Chem.* **1996**, *411*, 51.
(30) Schumacher, R. *Angew. Chem., Int. Ed. Engl.* **1990**, *29*, 329.
(31) Buttry, D. A. In *Electroanalytical Chemistry*; Bard, A. J., Ed.; Marcel Dekker: New York, 1990; Vol. 17, p 1.
(32) Ward, M. D.; Buttry, D. A. *Science* **1990**, *249*, 1000.
(33) Buttry, D. A.; Ward, M. D. *Chem. Rev.* **1992**, *92*, 1355.
(34) Hudson, B. S.; Ridyard, J. N. A.; Diamond, J. *J. Am. Chem. Soc.* **1976**, *98*, 1126.
(35) Yip, K. L.; Lipari, N. O.; Duke, C. B.; Hudson, B. S.; Diamond, J. *J. Chem. Phys.* **1976**, *64*, 4020.
(36) Logdlund, M.; Dannetun, P.; Stafstrom, S.; Salaneck, W. R.; Ramsey, M. G.; Spangler, C. W.; Fredriksson, C.; Bredas, J. L. *Phys. Rev. Lett.* **1993**, *70*, 970.
(37) Logdlund, M.; Bredas, J. L. *J. Chem. Phys.* **1994**, *100*, 6543.
(38) Itoh, T.; Kohler, E. *J. Phys. Chem.* **1988**, *92*, 1807.
(39) Spangler, C. W.; Nickel, E. G.; Hall, T. *J. Polym. Prepr.* **1987**, *28*, 219.
(40) Yamamoto, Y.; Aoyama, T.; Hayashi, K. *J. Chem. Soc., Faraday Trans.* **1988**, *84*, 2209.
(41) Aoyama, T.; Yamamoto, Y.; Hayashi, K. *J. Chem. Soc., Faraday Trans.* **1989**, *85*, 3353.
(42) Bally, T.; Roth, K.; Tang, W.; Schrock, R. R.; Knoll, K.; Park, L. Y. *J. Am. Chem. Soc.* **1992**, *114*, 2440, and references therein.
(43) Garnier, F.; Horowitz, G.; Peng, X.; Fichou, D. *Adv. Mater.* **1990**, *2*, 592.
(44) Hand, E. S.; Belmore, K. A.; Kispert, L. D. *Helv. Chim. Acta* **1993**, *76*, 1928; *Helv. Chim. Acta* **1993**, *76*, 1939; *J. Chem. Soc., Perkin Trans.* **1993**, *2*, 659.
(45) Shin, M.; Kim, E. Y.; Kwak, J.; Jeon, I. C. *J. Electroanal. Chem.* **1995**, *394*, 87.
(46) Grant, J. L.; Kramer, V. J.; Ding, R.; Kispert, L. D. *J. Am. Chem. Soc.* **1988**, *110*, 2155.

(47) Jeevarajan, A. S.; Kispert, L. D.; Wu, X. *Chem. Phys. Lett.* **1994**, *219*, 427.
(48) Sauerbrey, G. *Z. Phys.* **1959**, *155*, 206.
(49) Rubinstein, I.; Rishpon, J.; Redondo, A.; Gottesfeld, S. *J. Am. Chem. Soc.* **1990**, *112*, 6135.
(50) Rishpon, J.; Redondo, A., Derouin, C.; Gottesfeld, S. *J. Electroanal. Chem.* **1990**, *294*, 73.
(51) Shimazu, K.; Yanagida, M.; Uosaki, K. *J. Electroanal. Chem.* **1993**, *350*, 321.
(52) *HyperChem Version 4.0*; supplied by HyperCube, Inc., 419 Phillip St., Waterloo, Ontario, Canada N2L 3X2.
(53) Ehrenfreund, E.; Moses, D.; Heeger, A. J.; Cornil, J.; Bredas, J. L. *Chem. Phys. Lett.* **1992**, *196*, 84.
(54) Heeger, A. J.; Kivelson, S.; Schrieffer, J. R.; Su, W.-P. *Rev. Mod. Phys.* **1988**, *60*, 781.
(55) Jeevarajan, J. A.; Jeevarajan, A. S.; Kispert, L. D. *J. Chem. Soc., Faraday Trans.* **1996**, *92*, 1757.
(56) Bard, A. J.; Faulkner, L. R. *Electrochemical Methods: Fundamentals and Applications*, John Wiley & Sons: New York, 1980.
(57) *ChemPlus*; supplied by HyperCube, Inc., 419 Phillip St., Waterloo, Ontario, Canada N2L 3X2.